LBL-19442
Preprint c.2

Lawrence Berkeley Laboratory
UNIVERSITY OF CALIFORNIA

Materials & Molecular Research Division

RECEIVED
LAWRENCE
BERKELEY LABORATORY

JUN 4 1985

LIBRARY AND
DOCUMENTS SECTION

Submitted to Acta Metallurgica

A SIMPLE MODEL FOR THE PREDICTION OF COHERENT AND SEMICOHERENT PLATE PRECIPITATE HABIT PLANES

U. Dahmen and K.H. Westmacott

April 1985

TWO-WEEK LOAN COPY
This is a Library Circulating Copy
which may be borrowed for two weeks.

LBL-19442
c.2

Prepared for the U.S. Department of Energy under Contract DE-AC03-76SF00098

DISCLAIMER

This document was prepared as an account of work sponsored by the United States Government. While this document is believed to contain correct information, neither the United States Government nor any agency thereof, nor the Regents of the University of California, nor any of their employees, makes any warranty, express or implied, or assumes any legal responsibility for the accuracy, completeness, or usefulness of any information, apparatus, product, or process disclosed, or represents that its use would not infringe privately owned rights. Reference herein to any specific commercial product, process, or service by its trade name, trademark, manufacturer, or otherwise, does not necessarily constitute or imply its endorsement, recommendation, or favoring by the United States Government or any agency thereof, or the Regents of the University of California. The views and opinions of authors expressed herein do not necessarily state or reflect those of the United States Government or any agency thereof or the Regents of the University of California.

A Simple Model for the Prediction of Coherent and Semicoherent Plate Precipitate Habit Planes

U. Dahmen and K.H. Westmacott

National Center for Electron Microscopy
Materials and Molecular Research Division
Lawrence Berkeley Laboratory
University of California
Berkeley, CA 94720

Abstract

A quantitative physical description of the processes that determine plate precipitate habit planes evolves when a transformation with strains of mixed sign is modelled as a tensile test. The state of stress in such a thin coherent plate is similar to that in a tensile bar. The tensile axis, and with it the habit plane, is determined by the elastic anisotropy in the coherent case and by the slip geometry in the semicoherent case. The physical connection between the habit planes predicted by the anisotropic strain energy minimum criterion and the invariant plane strain criterion of martensite theory lies in the different constraints imposed by elastic or plastic yielding. Examples of the application of the principles and comparisons with experimental observations are given.

1. Introduction

The theoretical prediction of plate precipitate habit planes from first principles is a basic problem in materials science. Two distinctly different approaches are, the phenomenological theory of martensite transformations (1-5) and the theory of elastic inclusions (6-10). Martensite theory was formulated for diffusionless transformations but applications of its crystallographic principles

to diffusion-controlled precipitation reactions have often met with good success (11-20). Linear elastic theory is strictly valid only for small strains but many studies have applied the theory successfully to transformations with strains larger than 5% (21-34). In spite of the considerable overlap in the predictions of the two theories, only few efforts have been made to compare and contrast their basic assumptions (35,20).

The object of the present study is to develop a model of the physical principles underlying the formation of coherent and semicoherent precipitate plates, to apply its quantitative predictions to experimental observations, and to establish a connection between the two theories.

2. The coherent plate

The elastic strain energy of a very thin coherent disc-shaped inclusion is determined almost entirely by the components of the transformation strain in the plane of the disc (8,9). Thus an inclusion undergoing a transformation with principal strains e_1, e_1 and e_3 along the [100], [010] and [001] axes forming a thin plate on the (001) plane (Fig. 1(a)) has a strain energy of $W = 2\mu\frac{1+\nu}{1-\nu}e_1^2$ (8,9)(μ is the shear modulus and ν is Poisson's ratio). This expression is an approximation since it assumes that the precipitate aspect ratio c/a is infinitely small. Note that the strain energy depends only on the strain e_1 in the (001) plane. In this orientation the inclusion is like a thin elastic sheet under two-dimensional hydrostatic stress (Fig. 1(b)). However, since e_1 and e_3 are assumed here to have opposite sign, another orientation can be found leaving the plate in the simple state of uniaxial stress as for example in a tensile test. As shown below this

new orientation of the plate further reduces the strain energy.

Consider a plate that is inclined to the (001) plane to contain a direction in the interface in which the transformation strain is zero. Such a direction must exist since the strain changes sign between e_1 and e_3. This is shown in a schematic in Fig. 1(c) illustrating how a unit circle transforms to an ellipse by an expansion e_3 along [001] and a contraction e_1 along [100]. The angle θ of this unextended line with the (001) plane is given by $\tan\theta = \sqrt{-e_1/e_3}$. If a thin disc takes this orientation (see Fig. 2(d)) it is elastically distorted in its plane only by a uniaxial extension $-e_1$ (with corresponding stress σ, see Fig. 1(e)) constraining the transformation strain e_1, while the direction normal to it is free of transformation strain (unextended line).

This is the geometrical condition of an invariant (unextended and unrotated) line in the interface as it is used for instance in martensite theory (4). However, in the elastic case considered here a better approximation is that of a stress-free rather than a strain-free direction. The elastic strain $-e_1$ along the [010] axis causes a Poisson contraction νe_1, in the (010) plane. This is superimposed on the transformation strains in the (010) plane (shown in Fig. 1(c)), e_3 and e_1. Thus for a strain-free line $\tan\theta = \sqrt{\frac{e_1}{e_3}}$ while for a stress-free line $\tan\theta = \sqrt{-\frac{e_1(1+\nu)}{e_3+\nu e_1}}$. The latter expression is identical to Christian's solution (35) for the minimum strain energy. Since the strain energy is dominated by the uniaxial tension its magnitude is estimated simply as $W = \frac{1}{2} E e_1^2 = \mu (1+\nu) e_1^2$ (E is Young's modulus). This is only about one third of the energy ($W = 2\mu \frac{1+\nu}{1-\nu} e_1^2$)

of a plate on the (001) plane, i.e. one without inclination (Fig. 1(a)).

In an isotropic crystal the tensile stress constraining the plate could be in any direction in the (001) plane containing the uniform strain e_1. The final precipitate would be a plate inclined by $\theta°$ about this direction. In the preceding section this was chosen arbitrarily to be [010] see Fig. 1(d,e)). In an anisotropic crystal this tensile axis should lie in a soft direction in the (001) plane to lower the strain energy further. The problem of minimum strain energy is then reduced to finding the direction $\underline{p}$ in the (001) plane with the smallest Young's modulus. This direction will become the "tensile axis" in the stressed precipitate.

In general Young's modulus in the direction of unit vector $\underline{p}$ is $E(\underline{p}) = c_{ijkl}\, p_i p_j p_k p_l$ (36,37) where c_{ijkl} is the tensor of elastic constants and the summation convention is implied. For a cubic crystal, this simplifies to $E(\underline{p}) = c_{11} - (2c_{11} - 2c_{12} - 4c_{44})(p_1^2p_2^2 + p_2^2p_3^2 + p_3^2p_1^2)$ and since $p_3 = 0$ ($\underline{p}$ lies in the (001) plane) and $p_1^2 + p_2^2 = 1$ ($\underline{p}$ is a unit vector), $E(\underline{p}) = c_{11} - (2c_{11} - 2c_{12} - 4c_{44})\, p_1^2(1-p_1^2)$. The two extrema are at $p_1^2 = 1$ and $p_1^2 = \frac{1}{2}$, i.e. along the direction <100> or <110>. Which of these directions is the minimum depends on the sign of $(2c_{11} - 2c_{12} - 4c_{44})$, more commonly expressed through the anisotropy ratio $A = \frac{2c_{44}}{c_{11}-c_{12}}$. If $A > 1$, the <100> directions are soft and if $A < 1$, the <110> directions are soft. Since the tensile axis is contained in the habit plane and constitutes the axis of rotation for the plate the minimum energy habit plane is of the type {0kl} if $A>1$ and {hhl} if $A < 1$. The same prediction was made by Wen et al. (33) who obtained an exact solution for this case of tetragonal strains

using Khachaturyan's formulation of the elastic inclusion problem (10). They plotted the angle θ of the habit plane inclination as a function of the tetragonality ratio $\eta = (e_3 - e_1)/e_1$ and obtained the solid curve shown in Fig. 2.

Substitution in the simple geometrical approximation of a strain-free line given earlier yields $\tan\theta = \sqrt{-1/(\eta + 1)}$, which, when plotted, (dashed line) is seen to be within a few degrees of the exact result. (actually within the experimental error limits of coherent habit plane determinations). The more accurate approximation of a stress-free line leads to the expression $\tan\theta = \sqrt{-\frac{1+\nu}{\eta+1+\nu}}$. When plotted in Fig. 2 with $\nu = 1/3$, this superimposes on the solid line, i.e. is identical to the exact result even though an isotropic and average value for ν was assumed.

To summarize; an inclination of the plate forming an invariant line in the interface lowers the strain energy by about two thirds. The effect of elastic anisotropy is to select the axis of inclination. The predicted habit plane is {0kl} with $k/l \simeq \sqrt{e_1/e_3}$ if $A > 1$ and {hhl} with the same angle of inclination if $A < 1$. Since the strain energy is mainly due to the elastic distortion of the inclusion, A should be strictly the anisotropy ratio of the precipitate.

As shown in Fig. 3 this situation may be represented in a stereogram in an [001] orientation, i.e. the direction of the unique strain e_3. The habit plane is determined by the elastically soft tensile direction $\underline{p}$ in the (001) plane (either <100>, solid lines, or <110>, dashed lines) and an invariant line (more accurately a stress-free line) normal to it. This invariant line is simply the direction, normal to the tensile

axis $\underline{p}$, lying on the cone of unextended lines (4,17,19). Fig. 3 illustrates this for a crystal with an anisotropy ratio A>1, i.e. the tensile axis is [100]. The transformation strain in this example is characterized by $\eta \simeq -45$, i.e. the cone of unextended lines makes an angle of $\sim 9^\circ$ with the (001) plane. The (okl) habit plane normal is shown by a star and the invariant line by an open circle.

3. The semicoherent plate

The tensile test analogy can be carried further. Consider a thin plate in a state of uniaxial tension. If it deforms plastically it is most likely to do so on the slip system with the highest resolved shear stress. This depends on the relative position of the tensile axis and the slip system; and the resolved shear stress is a maximum if both the slip plane and the slip direction make an angle of 45° with the tensile axis. The problem of finding a direction in the (001) plane with a low Young's modulus in the elastic case now translates to finding the tensile direction in the (001) plane with the highest Schmid factor $R = \cos\phi \cos\lambda$ (where ϕ and λ are the angles of the tensile axis with the slip direction and the slip plane normal, respectively) for an available slip system. For a given slip plane the slip direction is linked to the tensile axis by the geometrical restriction of maintaining an unrotated and undistorted habit plane. The calculation of the slip direction is a lengthy process and as a first approximation it may be assumed that the Schmid factor is maximized when the tensile axis makes an angle of $\lambda = 45^\circ$ with the slip plane. For slip on the (101) plane this direction is [100], as shown in the stereogram in Fig. 4(a). The invariant line must be located at the intersection

of the cone of unextended lines with the slip plane so that it remains unaffected by the plastic deformation, a condition well-known from martensite theory. The resulting habit plane contains the [100] tensile axis and is therefore of the type (0kl) , where k and l are given by the invariant line condition. The similarity between this semicoherent case and the coherent case for A>1 is also apparent from the stereograms in Fig. 3 and 4.

If the slip plane is not one of the {101} planes inclined 45° to the (001) plane, but one of the {110} planes normal to (001) (see Fig. 4(b)) the tensile axis in the (001) plane, and at 45° to the (110) plane is again [100]. Again an (0kl) habit will result, but k and l are now given by the invariant line on the (110) rather than the (101) slip plane.

It must be kept in mind that even though the slip planes and the soft tensile axes are expressed in terms of crystal directions of the bcc matrix crystal, the important properties are those of the corresponding directions in the precipitate crystal. Thus the elastic constants or slip geometry in the precipitate determine the habit planes, and the discussion in terms of the bcc matrix is only a convenient tool.

4. Comparison with experimental observations

Experimental results for each of the three cases of uniaxial tension listed above are available. The transformation strains for bct α'' precipitates in Fe-N alloys are small enough to be in the coherent elastic range. The formation of fcc γ' precipitates in bcc Fe-N alloys constitutes an example of large transformation strains with slip occuring

on the inclined {101} bcc slip planes (see Fig. 4(a)). Hexagonal Mo_2C carbide in bcc Mo is a case of large transformation strains with slip on the vertical {110} bcc slip planes (Fig. 4(b)).

4.1 α" $Fe_{16}N_2$ (bct) in Fe (bcc)

The transformation strain is tetragonal (strictly cylindrically symmetric) and using the lattice parameters of Jack (38), $\epsilon_{ij} = \begin{pmatrix} -0.0023 & & \\ & -0.0023 & \\ & & 0.0971 \end{pmatrix}$. Since the anisotropy ratio A, is greater than unity for Fe the habit plane predicted for α" is (okl) with k/l $\simeq \frac{0.0023}{0.0971}$, a plane that is inclined about 8.5° with respect to (001). Hong et al. (39) have calculated a strain energy minimum for (001) plates with aspect ratio less than 11.35. A recent TEM analysis (40) has shown that each α" particle is made up of thin segments inclined about 10° with respect to (001). Several such segments, inclined about different axes form a puckered sheet giving the typical rosette contrast in TEM (Fig. 5). The overall habit of the puckered sheet is (001). However, the anisotropy predicted by the tensile direction with the lowest Young's modulus was not observed here, although evidence exists to suggest a directionality occurs when α" is formed at low aging temperature (41). Experimental observations thus confirm the predicted rotation required to form a stress-free line in the interface. But instead of a single plate with {okl} habit a further reduction in energy is apparently achieved by grouping several variants in a puckered sheet arranging their tensile axes in a star-like pattern.

4.2 γ' Fe_4N (fcc) in Fe (bcc)

As for α" $Fe_{16}N_2$, the transformation strain is tetragonal. Using the lattice parameters at the aging temperature of 300°C, a_{bcc} = 0.28678

nm, a_{fcc} = 0.3795 nm, we obtain $\varepsilon_{ij} = \begin{pmatrix} -0.0643 & & \\ & -0.0643 & \\ & & 0.3233 \end{pmatrix}$. These strains are large and the habit plane must be determined by the criterion of maximum Schmid factor. γ' slips on {111} fcc planes derived from the inclined {101} bcc slip planes. Hence this is the case illustrated in Fig. 4(a).

The predicted (okl) habit plane defined by the [-0.38, 0.85, 0.38] invariant line and the [100] tensile axis is (0,-0.41,0.91). To test that [100] was indeed the tensile axis in the (001) plane with the highest resolved shear stress, other nearby (hkl) habit planes were calculated using Ledbetter and Wayman's computer program for martensite crystallography (42). The Schmid factor was confirmed to be a maximum for the [100] axis.

The predicted (0,-0.41,0.91) habit agrees exactly with the experimental observations (43). Fig. 6(a) shows a TEM image of a typical γ' plate. The parallel striations are interfacial dislocations along the invariant line direction. Often two sets of striations are found within a single plate. As detailed elsewhere (43) this means that the habit plane is of the type {okl}, i.e. it contains a <100> direction. Usually two variants form in a V-shaped grouping, and the habit plane can thus be measured accurately from the angle of inclination (42°) between the two variants. The slip plane is the required {111} fcc plane as evidenced by the <111> streaking seen in electron diffraction patterns of extracted plates (43,44) Fig. 6(b)).

4.3 Mo_2C (hcp) in Mo (bcc)

A further test of the concept is found in the formation of semicoherent plates of Mo_2C (hcp) in Mo (bcc). Using the lattice

parameters a_{bcc} = 0.3147 nm, a_{hcp} = 0.3002 nm, c_{hcp} = 0.4724 nm, the transformation strain tensor is:

$$\varepsilon_{ij} = \begin{pmatrix} 0.17 & & \\ & 0.06 & \\ & & -0.05 \end{pmatrix}.$$

when referred to [110], [1$\bar{1}$0] and [001] axes (45). In the Pitsch-Schrader lattice correspondence (16,45) these directions transform to [0001], [01$\bar{1}$0] and [2$\bar{1}\bar{1}$0], respectively. Fig. 7 shows that since all three principal strains are different the cone of unextended lines now has an elliptical cross section. Due to the crystallography of the hexagonal Mo_2C precipitate, (0001) is the slip plane. This is derived from the vertical (110) bcc slip plane, corresponding to the case shown in Fig. 4(b). Again, the tensile axis in the (001) plane (the plane of unmixed strains) at 45° to the (110) bcc / (0001) hcp slip plane is [100]. The invariant line at the intersection of the cone of unextended lines with the (110) slip plane is ∿[$\bar{1}$13]. The resulting (0kl) habit plane containing the [100] tensile axis and the [$\bar{1}$13] invariant line is (0$\bar{3}$1), indicated by a star in Fig. 7. Again, this agrees with the experimental observations (Fig. 8) showing an Mo_2C carbide plate with [113] interfacial dislocations, (0$\bar{3}$1) habit and slip on (0001) hcp / (110) bcc planes (45).

As in the example of γ' Fe_4N above, the habit plane with the tensile axis of maximum Schmid factor was also calculated exactly by systematically varying the slip direction while keeping the slip plane constant. The tensile axis so determined was 1.5° from [100], close enough to make an experimental distinction in small plates impossible. Within experimental accuracy the assumed [100] tensile axis is thus the direction in the (001) plane with maximum Schmid factor.

5. Discussion

In the three cases considered here the tensile test analogy yields simple and accurate predictions for precipitate habit planes. The tensile axis must be a soft direction in the plane of unmixed strain - in our examples the (001) plane. For coherent precipitates the tensile axis must be elastically soft, i.e. have a low elastic modulus, and for semicoherent precipitates it must be plastically soft, i.e. be oriented for the maximum Schmid factor on the slip system. In all three cases considered the tensile axis is very close to <100> and the resulting habit plane is {0kl}, where k and l are given by the invariant line condition.

Not only does the tensile test analogy describe the transition from coherent to semicoherent inclusions physically as the change from elastic to plastic yielding, it also allows a remarkably simple and accurate prediction of coherent and semicoherent precipitate habit planes. At first glance, this simplicity is in contrast to the more complicated habit plane calculations of martensite theory (5). However, a closer examination shows the irrational {hkl} habit planes predicted by martensite theory result from the geometrical constraints imposed by assuming rational slip elements (e.g. $(101)/[\bar{1}01]$). The assumption in the present analysis that [100] is the optimum tensile axis gives a simple (0kl) form to the habit plane. But the necessary slip direction in the low-index slip plane is irrational and as lengthy to calculate as the irrational habit plane with low-index slip elements. The apparent simplicity stems from the fact that the (irrational) slip direction is only of secondary importance for the habit plane determination.

The habit plane is fully prescribed by the invariant line at the intersection of the cone of unextended lines with the slip plane and by the tensile axis. The Schmid factor is expected to be large for a tensile axis at 45° to the shear plane. The tensile axis must also lie in the plane of unmixed principal strains, the (001) planes in the three examples given. Thus [100] is the tensile axis and (0kl) the habit plane only to first approximation. In order to calculate exactly the direction in the (001) plane for which the Schmid factor is a maximum, the slip direction must also be known accurately and thus the entire calculation must be carried out exactly as for martensite with an irrational {hkl} habit plane (42).

In the case of Fe_4N γ' in Fe it was found that [100] is indeed the direction of maximum Schmidt factor. For Mo_2C in Mo the maximum occurs in a direction less than 1.5° from [100]. Considering experimental errors inherent in the determination of habit planes of small plates, e.g. the fact that they are often wedge-shaped instead of plane parallel in cross section (43,45,46), the use of [100] as the direction with the highest resolved shear stress on the slip system is justified. The orientation relationships calculated for [100] tensile axes and slip on the inclined (101) planes for $\gamma'Fe_4N$ and on the vertical (110) planes for Mo_2C also agree with those measured experimentally (43,45). It appears from these limited data that a 45° angle to the slip plane is a good approximation for the tensile axis if the slip plane is rational and the slip direction irrational.

The use of an irrational slip direction with a rational slip plane is not new. Crocker and Bilby (47) explored various such combinations

by using a double shear model for the lattice invariant deformation in martensite theory, for example by allowing two different slip directions (Burgers vectors) on a single slip plane. As a criterion for optimization they used the smallest minimum of the shape shear m_1 and of the lattice invariant shear m_2. The shear m_2 is directly related to the density of interfacial (anticoherency) dislocations (48,49) and m_1 relates to the energy of accommodation of the semicoherent plate.

It is instructive to compare the present criterion of maximum Schmid factor to the minimum in shape shear m_1 and lattice invariant shear m_2. In the case of γ' Fe_4N the minimum shape shear m_1 occurs for a $[\bar{1}01]$ slip direction, the minimum lattice invariant shear m_2 for a [-0.66, 0.36, 0.66] direction and the maximum Schmid factor for the direction [-0.69, 0.22, 0.69], which lies between the minimum for m_1 and m_2. The corresponding habit planes range over 7.2°.

In Mo_2C precipitates the minimum for both m_1 (0.29) and m_2 (0.18) lie at the rational slip direction $[1\bar{1}0]$. The maximum Schmid factor criterion requires [0.68, -0.68, 0.26] to be the slip direction with m_1 = 0.31 and m_2 = 0.21. The corresponding habit planes are 10.6° apart. It thus appears that optimization of the tensile axis takes precedence over both m_1 and m_2 minimization although the latter deviations are quite small.

Bowles and Tegart (11) and Otte and Massalski (12) have applied martensite crystallography to nucleation-and-growth transformations, assuming rational shear elements. However no fine scale TEM observations existed at the time to allow an exact comparison of theory with localized

microstructure, and the small discrepancies between theory and available data were discussed in terms of irrational shear elements and a dilatation parameter.

Finally, it is interesting to note that throughout it was assumed that the lattice invariant shear occurs in the inclusion rather than the matrix. Mathematically there is no difference whether the lattice invariant deformation occurs before or after the transformation, but physically there is a clear distinction. The faulting observed on the slip planes of Fe_4N and Mo_2C is clear evidence for slip within the particle even though the matrix is much softer. The faulting also allowed a clear identification of the operating slip plane.

Quite a different result was found in a recent study of needle-shaped precipitates in Cu-Cr (fcc/bcc) and Fe-Cu (bcc/fcc) alloys (19). Here the crystallography of the matrix slip planes was the determining factor. The needles in both alloys were found to lie along the invariant lines formed by the intersections of the cone of unextended lines with the matrix slip planes. A likely interpretation of this difference is that due to the different states of stress in needles and plates (needles are more complex) plastic accommodation occurs within the plates but in the matrix surrounding the needles.

6. Summary and Conclusions

By recognizing that at its minimum strain energy orientation a thin coherent plate precipitate with tetragonal transformation strains of mixed sign is approximately in a state of uniaxial stress, its optimum orientation in an elastically anisotropic cubic matrix becomes simple to predict from first principles. The habit plane must contain a stress-free line (approximately a strain-free, or invariant, line)

and an elastically soft direction in the plane of unmixed principal strains, and will therefore be of the type {0kl} if A>1 or {hhl} if A<1. The inclination θ of the habit plane with respect to the plane of unmixed principal strains is given by the ratio of the mixed principal strains $\tan\theta = \sqrt{-\frac{e_1}{e_3}}$

The transition from a coherent to semicoherent plate is modelled after a tensile test providing a physical picture of the connection between the theory of elastic inclusions and martensite theory. Loss of coherency (the lattice-invariant shear of martensite theory) occurs in the precipitate on a rational slip plane in an irrational direction with the tensile axis being a "plastically soft" direction in the plane of unmixed principal strains, i.e. the direction with the highest Schmid factor on the slip system.

Comparison with experimental results on habit planes and orientation relationships of three different alloy systems agree well with the model. To within experimental accuracy, in all three alloys the predicted tensile axis is <100> and the predicted and observed habit planes are of the type {0kl}.

Acknowledgements

We greatly appreciate the assistance of Dr. R. Kilaas with the Ledbetter/Wayman computer program on martensite crystallography a printout of which was kindly provided by Dr. Wayman. This work is supported by the Director, Office of Energy Research, Office of Basic Energy Sciences, Materials Sciences Division of the U.S. Department of Energy under Contract No. DE-AC03-76SF00098.

REFERENCES

1). M.S. Wechsler, D.S. Lieberman and T.A. Read, Trans. AIME 197, 1503 (1953).

2). J.S. Bowles and J.K. Mackenzie, Acta Met. 2, 129 (1954).

3). J.K. Mackenzie and J.S. Bowles, Acta Met. 2, 138 (1954).

4). C.M. Wayman, "Introduction to the crystallography of martensitic transformations," MacMillian, N.Y. (1964).

5). A.G. Crocker, J. De Physique, Coll. C4, 43 Suppl., p.C4-209, (1982).

6). J.D. Eshelby, Proc. Roy. Soc. (A) 241, 376 (1957).

7). J.D. Eshelby, Prog. Solid Mechanics 2, 89 (1961).

8). J.W. Christian, "The theory of tranformations in metals and alloys," Pergamon Press, NY (1965).

9). T. Mura, "Micromechanics of defects in solids", Martinus Nijhoff Publishers, Boston (1982).

10). A.G. Khachaturyan, "Theory of Structural Transformations in Solids", J. Wiley, New York (1983).

11). J.S. Bowles and W.J. McG. Tegart, Acta Met. 3, 590 (1955).

12). H.M. Otte and T.B. Massalski, Acta Met. 6, 494 (1958).

13). R. Smith and J.S. Bowles, Acta Met. 8, 405 (1960).

14). G.C. Weatherly, Acta Met. 29, 501 (1981).

15). V. Perovic, G.C. Weatherly and C.J. Simpson, Acta Met. 31, 1381 (1983).

16). U. Dahmen, Acta Met. 30, 63 (1982).

17). A. Crosky, P.G. McDougall and J.S. Bowles, Acta Met. 28, 1495 (1980).

18). A. Crosky, P.G. McDougall and J.S. Bowles, Acta Met. 31, 603 (1983).

19). U. Dahmen, P. Ferguson and K.H. Westmacott, Acta Met. 32, 803 (1984).

20). U. Dahmen and K.H. Westmacott, Proc. Conf. Solid-Solid Phase Transformations, Pittsburgh, (1981), p. 433.

21). M. Shibata and K. Ono, Acta Met. 23, 587 (1975).

22). T. Mura, T. Mori and M. Kato, J. Mech. Phys. Solids, 24, 305 (1976).

23). D.R. Clarke, Met. Trans. 7A, 723 (1976).

24). G.B. Olson and M. Cohen, Met. Trans. 7A, 1897 (1976).

25). K.E. Easterling and A.R. Tholen, Acta Met. 24, 333 (1976).

26). J.K. Lee, D.M. Barnett and H.I. Aaronson, Met. Trans. 8A, 963 (1977).

27). M. Shibata and K. Ono, Acta Met. 25, 35 (1977).

28). G.C. Weatherly, P. Humble and D. Borland, Acta Met. 27, 1815 (1979).

29). M. Suezawa and H.J. Cook, Acta Met. 28, 423 (1980).

30) K.E. Easterling and A.R. Tholen, Acta Met. 28, 1229 (1980).

31). W.E. Mayo and T. Tsakalakos, Met. Trans 11A, 1637 (1980).

32). D. Lepski and P. Burck, Phys. stat. sol. (9) 64, 625 (1981).

33). S.H. Wen, E. Kostlan, M. Hong, A.G. Khachaturyan and J.W. Morris, Jr., Acta Met. 29, 1247 (1981).

34). M. Hayakawa and M. Oka, Acta Met. 32, 1415 (1984).

35). J.W. Christian, Suppl. Trans. JIM 17, 21 (1976).

36). J.F. Nye, "Physical properties of crystals", Oxford University Press (1957).

37). Yu. I. Sirotin and M.P. Shaskolskaya, "Fundamentals of Crystal Physics", Mir Publishers, Moscow (1982).

38). K.H. Jack, Proc. Roy. Soc. 208A, 216 (1951).

39). M. Hong, D.E. Wedge and J.W. Morris, Jr., Acta Met. 32, 279 (1984).

40). P. Ferguson, U. Dahmen and K.H. Westmacott, Scr. Met. 18, 57 (1984).

41). Y.C. Shih, M.S. Thesis, U.C. Berkeley (1982), LBL Report Number 14284.

42). H.M. Ledbetter and C.M. Wayman, Mater. Sci. Eng. 7, 151 (1971).

43). U. Dahmen, P. Ferguson and K.H. Westmacott, to be published.

44). G.R. Booker, Acta Met. 9, 590 (1961).

45). J.M. Lang, U. Dahmen and K.H. Westmacott, Phys. stat. sol. (a)75, 409 (1983).

46). J.A. Klostermann, J. Less-Common Met. 28, 75 (1972).

47). A. G. Crocker and B.A. Bilby, Acta Met. 9, 678 (1961).

48). G.B. Olson and M. Cohen, Acta Met. 27, 1907 (1979).

49). G.B. Olson, Acta Met. 29, 1475 (1981).

FIGURE CAPTIONS

Fig. 1. (a) Thin plate precipitate on the (001) plane and (b) its state of two-dimensional hydrostatic stress. (c) the transformation strain is depicted schematically in the [010] projection with unextended lines at an angle θ to the (001) plane. In its optimum orientation (d) the thin plate is inclined and contains an invariant line in the interface. Its state of uniaxial stress along [010] is illustrated in (e).

Fig. 2. Plot of predicted angle θ of plate inclination vs. tetragonality ratio $\eta = (e_3-e_1)/e_1$. The dashed curve shows the strain-free (invariant) line approximation while the solid curve represents the exact result (33) and the stress-free line approximation.

Fig. 3. [001] stereogram illustrating the predicted habit plane (solid great circle) for anisotropy ratio A>1 and tetragonality ratio $\eta \simeq -45$. The pole of the (0k1) habit plane is marked by a star, the invariant line by an open circle. The elastically soft directions in the (001) plane are shown as solid lines along [100] and [010] (A>1) and dashed lines along [110] and [$1\bar{1}0$] (A<1).

Fig. 4. [001] stereograms showing habit planes determined by the [100] "tensile axis" and the invariant line (open circle) at the intersection of the cone of unextended lines with the inclined (101) slip plane in (a) and the vertical (110) slip plane in (b). The habit plane poles are marked by a star.

Fig. 5. Rosette contrast typical of bct α'' $Fe_{16}N_2$ particles in bcc Fe-N alloy.

Fig. 6. (a) Inclined plate of fcc γ' Fe_4N in bcc Fe showing interfacial lines (see arrows) along invariant line directions. The <110> selected area diffraction pattern (b) from an extracted γ' particle shows <111> streaking due to faults resulting from slip on {111} planes.

Fig. 7. [001] stereogram with an elliptical cone of unextended lines for hcp Mo_2C in bcc Mo with the invariant line (open circle) at the intersection of the cone with the (110)/(0001) slip plane. The (0kl) habit plane pole and trace are shown as a star and a solid great circle.

Fig. 8. (a) Inclined plate of hcp Mo_2C in bcc Mo showing interfacial lines along invariant line direction (see arrows). The diffraction pattern in (b) shows streaking of the precipitate reflections in the [0001] direction (see arrow) associated with faults due to slip on (0001) slip planes (45).

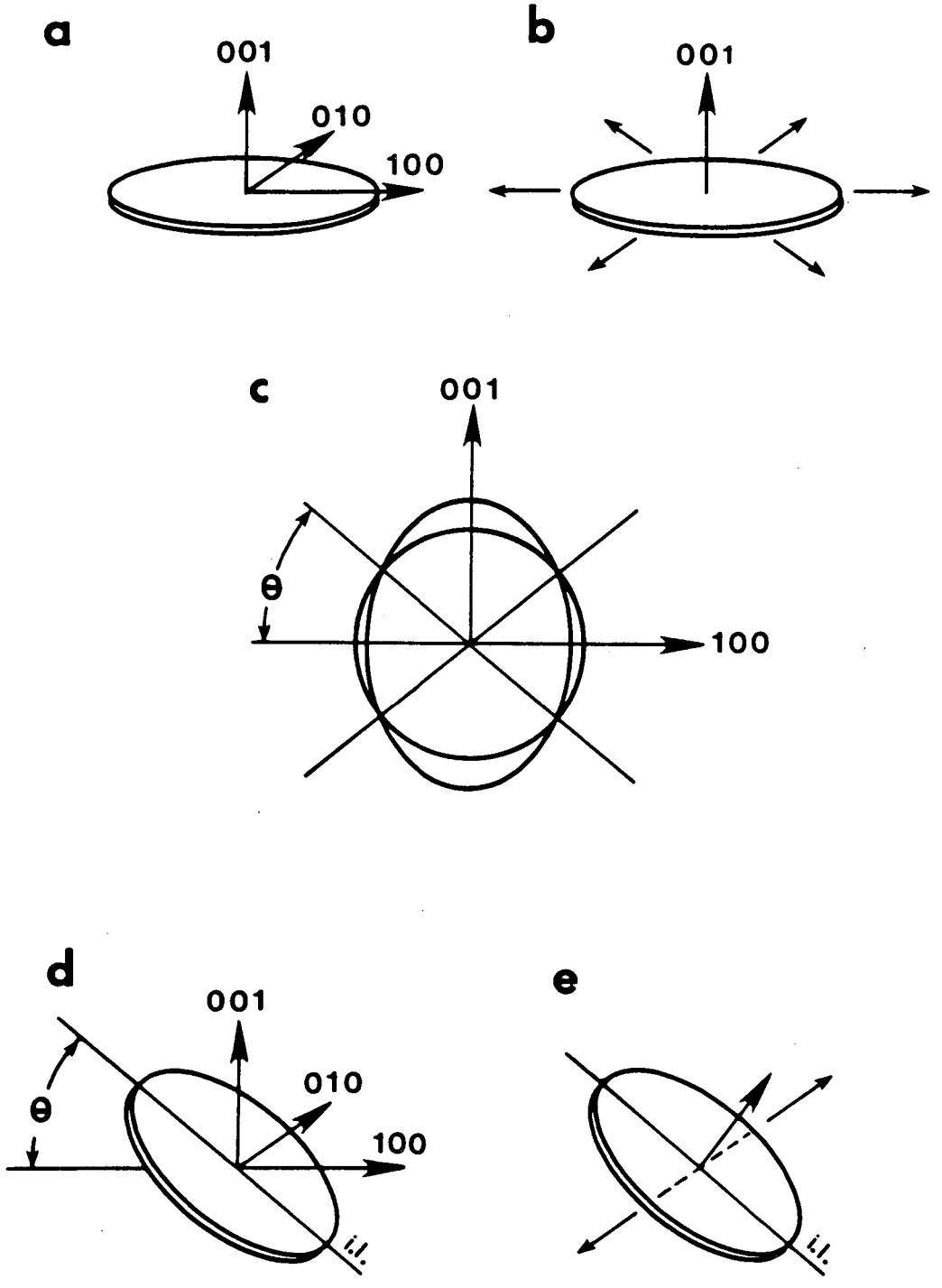

XBL 854-2117

Fig. 1

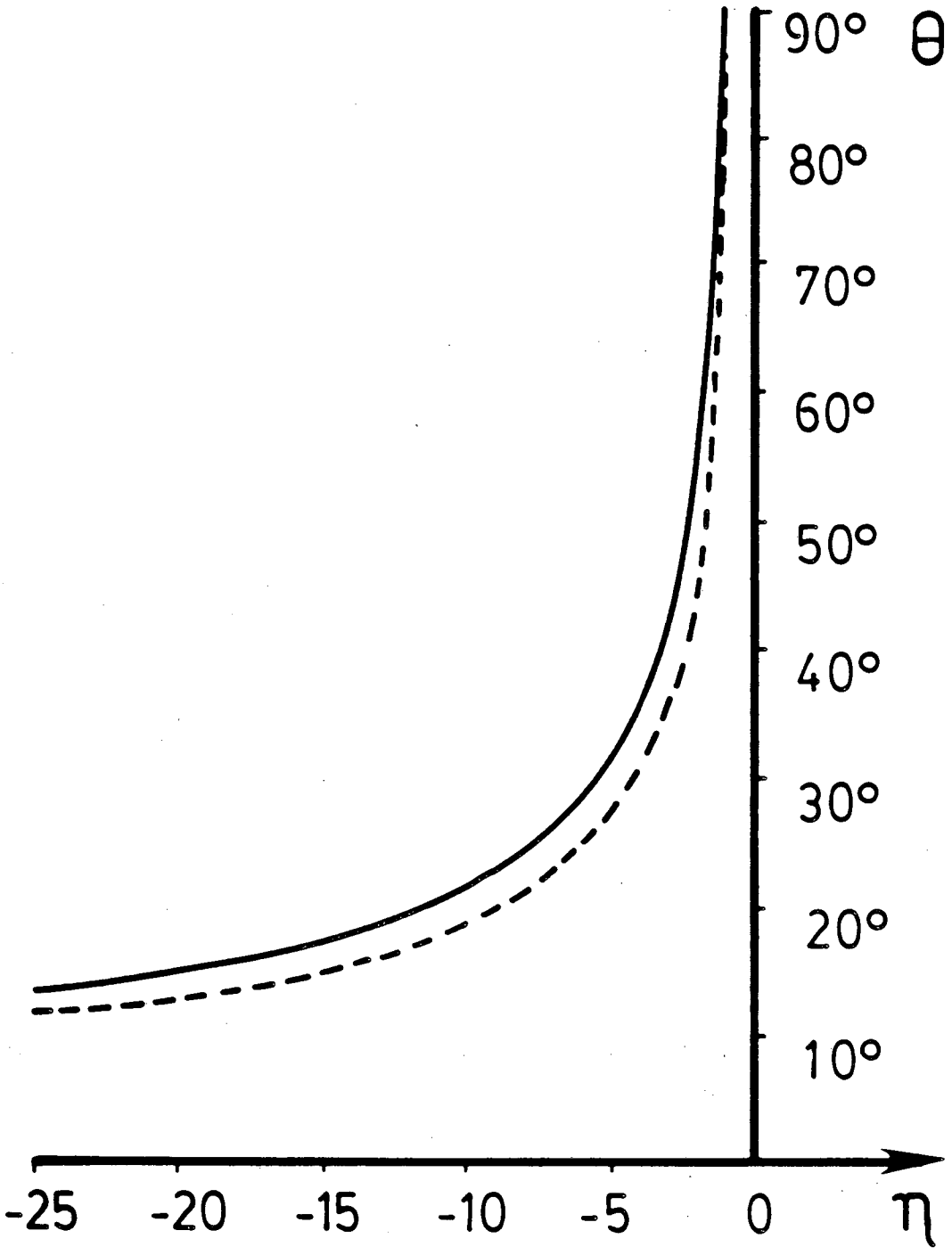

XBL 854-2118

Fig. 2

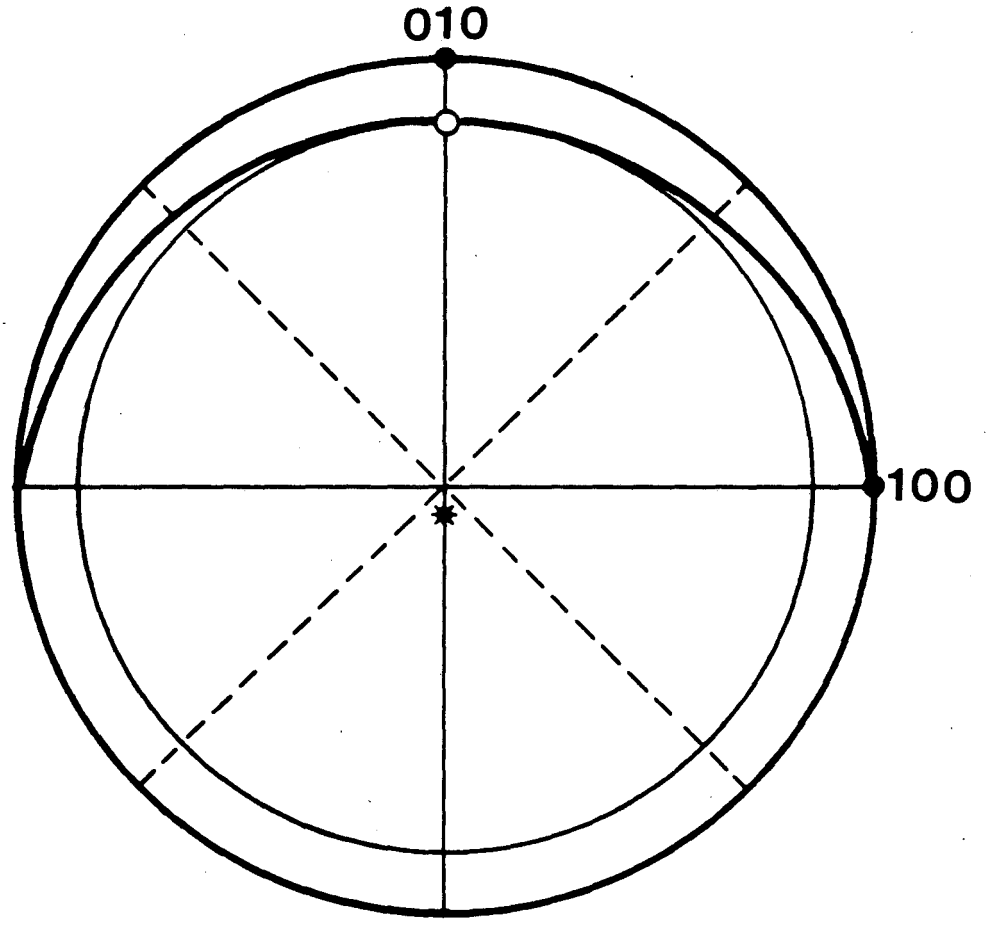

XBL 854-2119

Fig. 3

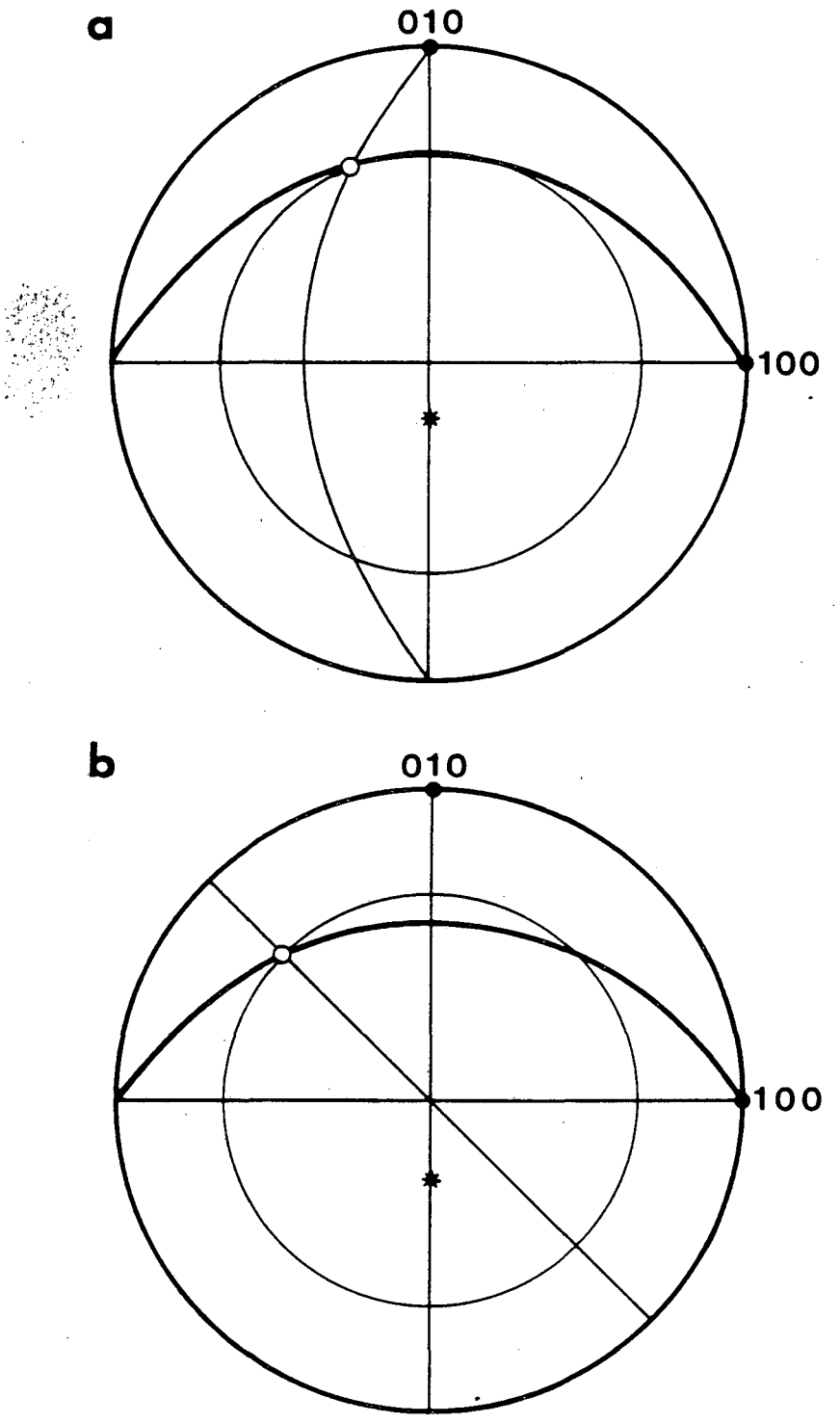

XBL 854-2120

Fig. 4

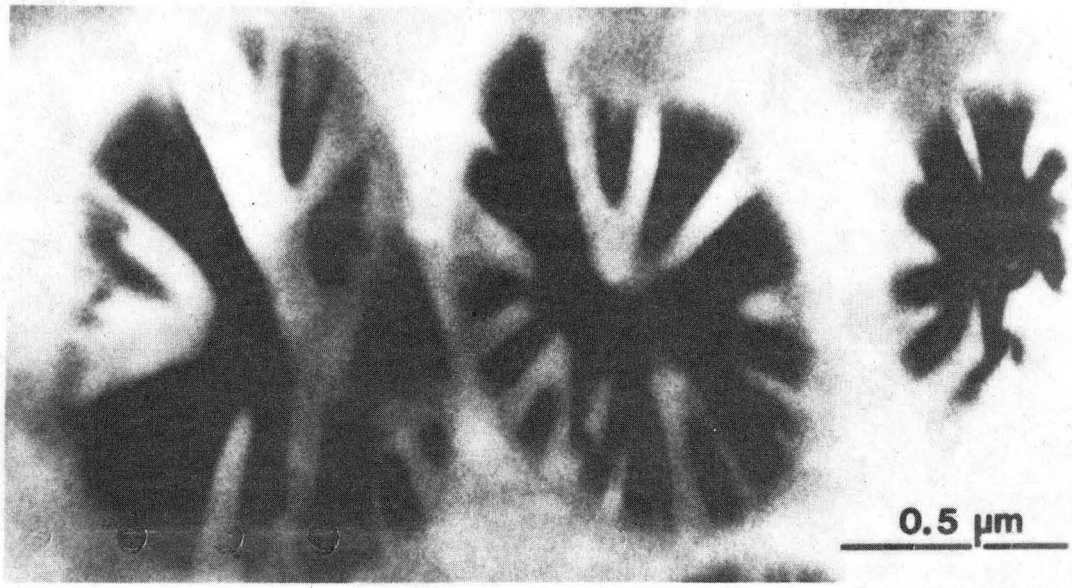

XBB 854-3097

Fig. 5

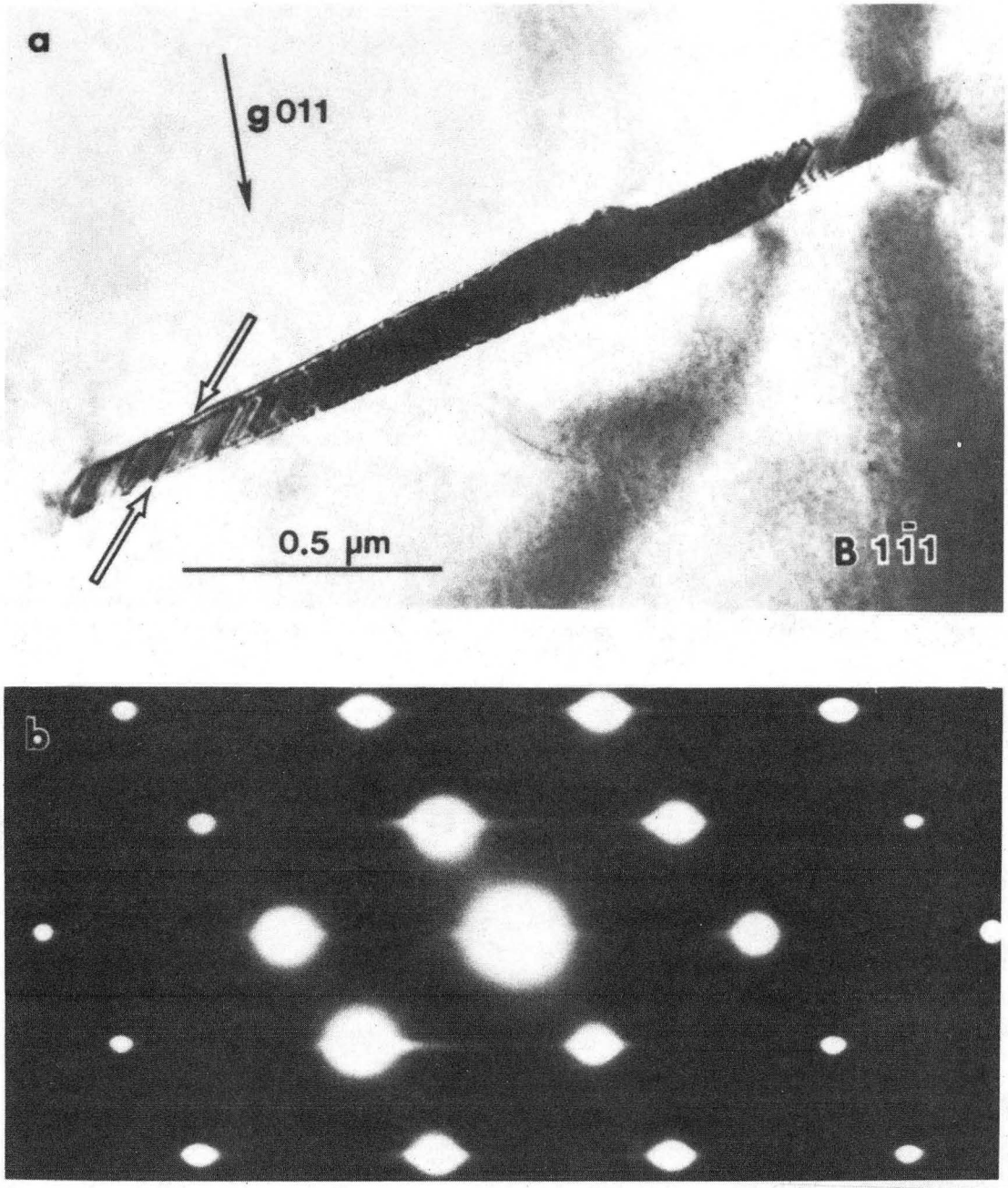

XBB 854-3099

Fig. 6

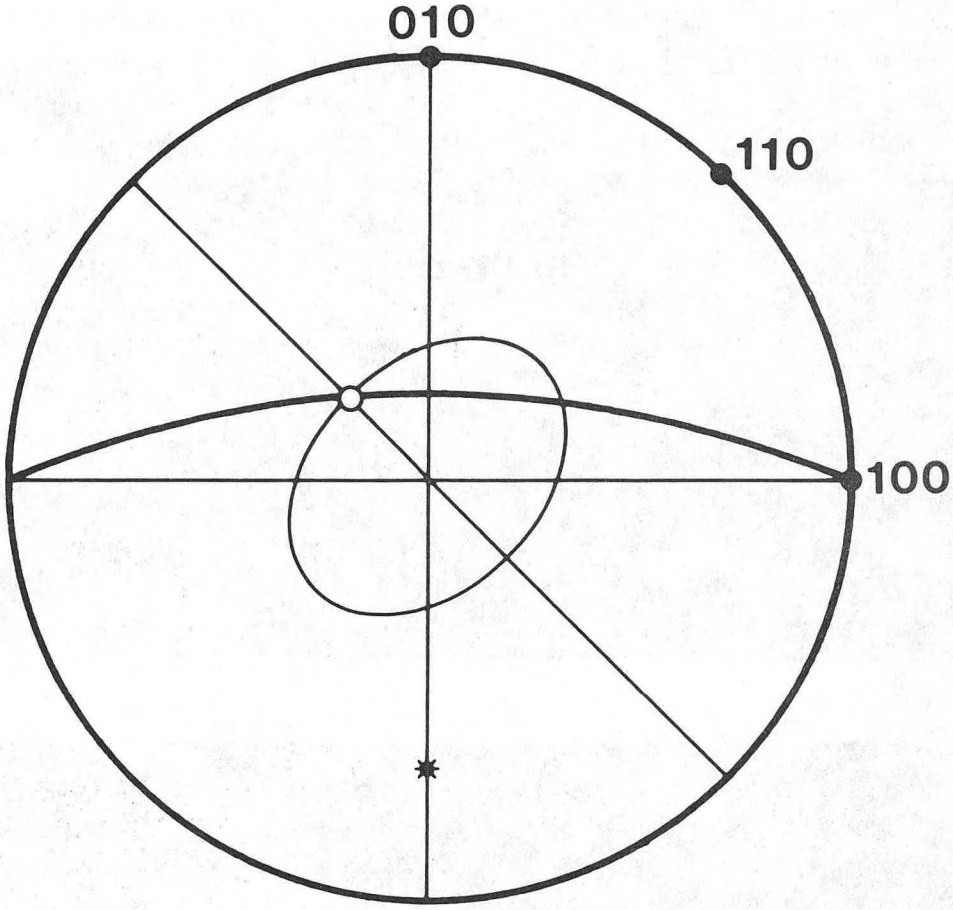

XBL 854-2121

Fig. 7

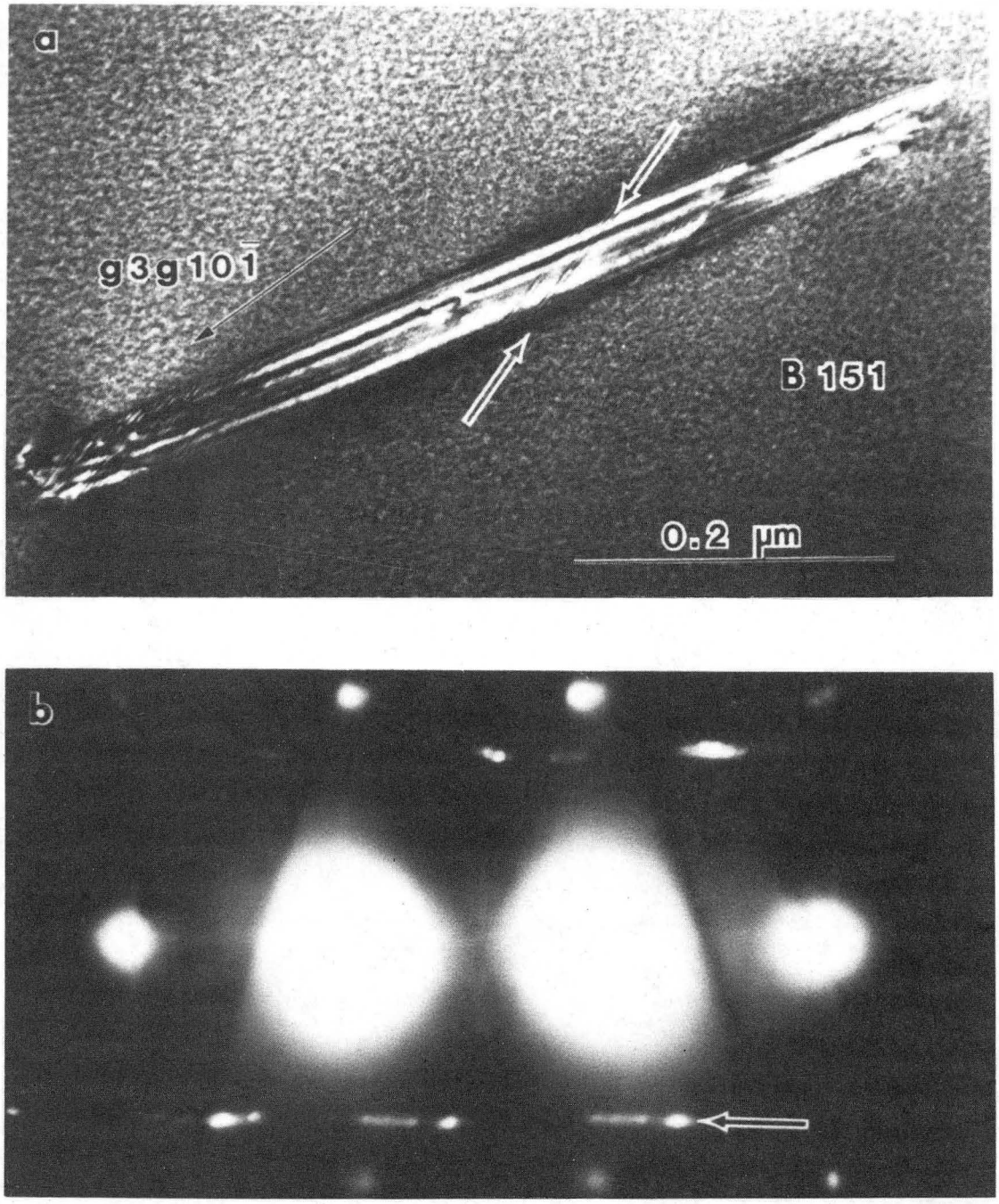

XBB 854-3098

Fig. 8

This report was done with support from the Department of Energy. Any conclusions or opinions expressed in this report represent solely those of the author(s) and not necessarily those of The Regents of the University of California, the Lawrence Berkeley Laboratory or the Department of Energy.

Reference to a company or product name does not imply approval or recommendation of the product by the University of California or the U.S. Department of Energy to the exclusion of others that may be suitable.

LAWRENCE BERKELEY LABORATORY
TECHNICAL INFORMATION DEPARTMENT
UNIVERSITY OF CALIFORNIA
BERKELEY, CALIFORNIA 94720